Simulation of Hollow Embossing Rolling for Bipolar Plate Forming using LS-DYNA©

Franz Reuther[1], Verena Psyk[1], Verena Kräusel[1], Martin Dix[1]

[1]Fraunhofer Institute for Machine Tools and Forming Technology IWU, Chemnitz

Abstract

Hollow embossing rolling constitutes a promising forming technology for metallic bipolar plates due to the high achievable production rates. The simulation-based process optimization is impeded by the incremental forming character and modeling of fine channel structures, which leads to large model sizes and computation times. This paper presents a shell-based finite element modeling approach using LS-DYNA© for bipolar plate forming simulation. Essential boundary conditions of the modeling are discussed, and recommended setting parameters are derived.

Keywords: hollow embossing rolling, roll forming, simulation, fuel cell, bipolar plate

1 Introduction

Expanding the use of hydrogen presents an excellent opportunity for reducing pollutant emissions and promoting hydrogen as a secondary energy carrier, especially in the context of the energy turnaround [1]. Electrolyzers and fuel cell stacks, which are used as electrochemical energy converters, contain multiple bipolar half plates (BPHP), which are essential components for media distribution. Ensuring high-volume production is necessary to make fuel cell technology available to the mass market [2]. Metallic BPHP can be produced by a variety of technological methods, such as hydroforming [3] and hollow stamping [4], which differ in terms of the production rates that can be achieved [5]. The possibility of mass-producing BPHP at lower costs and higher efficiency has driven the development of rolling processes in recent years. These processes can also incrementally shape channel structures in thin strips [5]. Several basic research papers have been published on this topic regarding roll forming of channel geometries, which are typical for BPHP [6, 7]. However, these approaches are limited to continuous channel geometries. Bauer et al. [8] first described the forming of discontinuous channel structures by hollow embossing rolling, demonstrating its potential for incrementally forming typical BPHP flow field designs for industrial applications. Further research activities provided initial approaches for forming process optimization based on FE simulations [9]. However, continuous further development of hollow embossing rolling is required to enable future series production of BPHP in common sizes and featuring typical flow field designs [10].

Efficient modeling and simulation of the forming process is an essential tool for gaining comprehensive understanding of the process, which is essential for optimization. The main challenges here arise from the incremental forming character and the resulting long calculation times. In addition, the sub-millimeter scale and thin metal strips (0.05 – 0.10 mm) require delicate channel structures, which demand a high level of precision in meshing the strip section and tools, resulting in a large number of elements. Therefore, FE simulation modeling is commonly limited to highly simplified BPHP geometries [11]. Preliminary attempts to simulate industry-standard plate designs result in excessive computing times [12], hindering process optimization through forming simulation. To address these shortcomings, this paper introduces a shell-based finite element model in LS-DYNA© to model the hollow embossing rolling process of bipolar half plates used in fuel cell applications efficiently. To this end, various modeling approaches are compared on a BPHP test geometry, and model errors, as well as possible reductions in computation time, are discussed.

2 Model setup of hollow embossing rolling using a small test geometry

A small BPHP test geometry was created for simulation studies, using common flow field designs and cross-section geometries [10] as references (Fig. 1a). The design considers geometric discontinuities that are common in real-size plate designs for automotive applications (such as changing channel orientations, channel arcs, and step-shaped transitions).

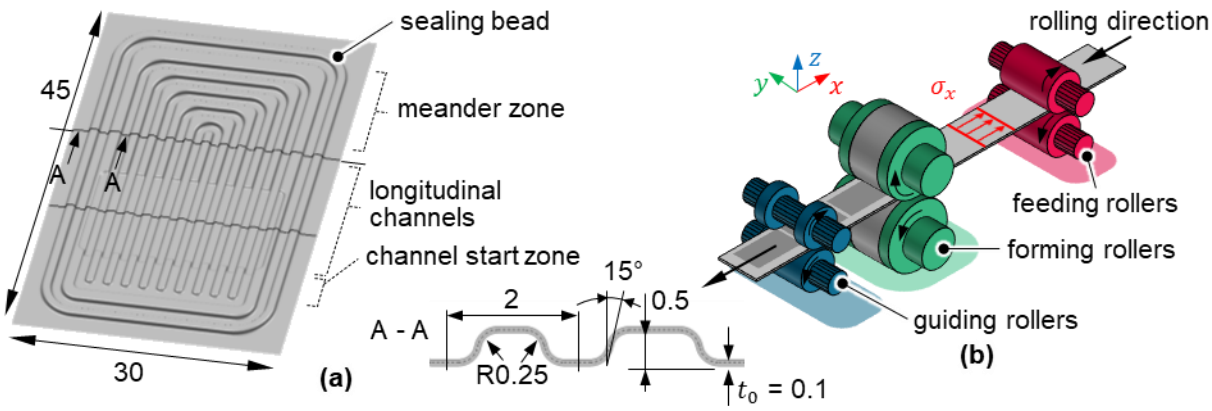

Fig.1: Boundary conditions for model development: (a) BPHP demonstrator, (b) process realization concept.

The FE model design for hollow embossing rolling is based on the process concept illustrated in Figure 1b. Initially, the strip passes through feeding rollers that generate a braking torque to create tensile stress σ_x in the strip. This is technologically necessary to prevent wrinkling in edge areas caused by uncontrolled longitudinal draw-in at the inlet side. After the incremental forming of the channel structure during the second rolling stage, guiding rollers guarantee safe transportation of the strip. A first explicit forming simulation model was created in the FE software LS-DYNA© R12.1 mpp, as shown in Figure 2a. The geometries of the forming rollers with a diameter of D = 105 mm were represented as rigid shell meshes rotating around a fixed turning point at a rotational speed of 20 rpm. This leads to a strip velocity of v_{real} = 110 mm/s. A target rolling gap s_{w0} that corresponds to the initial strip thickness of t_0 = 0.10 mm was considered between the roller surfaces. To make use of symmetry, only half of the 30 mm wide strip was meshed in the forming area with a uniform element edge length of 0.075 mm (no adaptivity), resulting in a total of 110,000 elements (Fig. 2b).

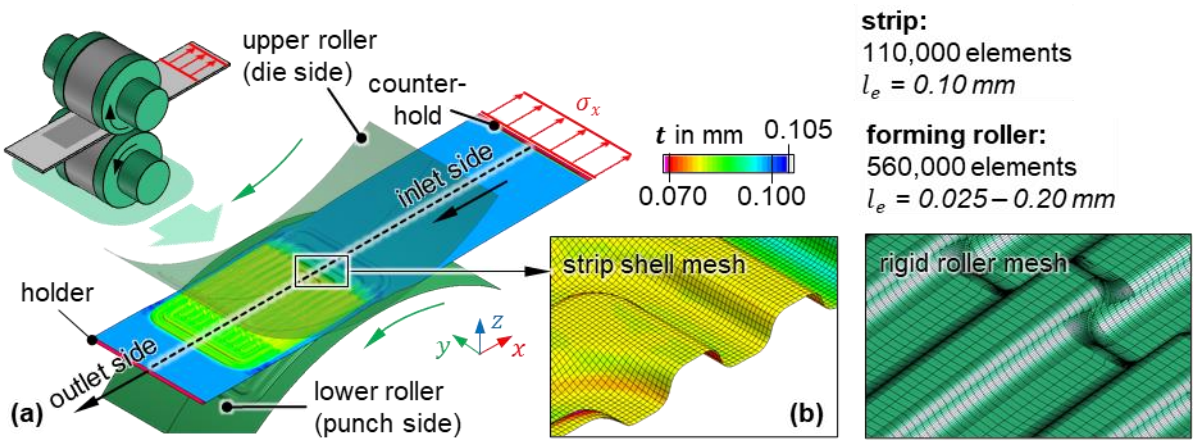

Fig.2: Modeling of hollow embossing rolling: (a) forming simulation model, (b) boundary conditions for tool and strip meshing.

The strip was discretized using common Belytschko-Lin-Tsay shell element types (ELFORM = 2) for forming simulation in LS-DYNA with three integration points across the thickness (n_{IP} = 3). Furthermore, the model includes two rigid bodies at the strip ends enabling the implementation of a translational constraint on the strip outlet side in synchronization with the roller rotation (***BOUNDARY_PRESCRIBED_MOTION_RIGID**) as well as tensile stress application (σ_x) by a force controlled counterhold (***LOAD_RIGID_BODY**). In the initial approach, a conservative Coulomb friction model with a static friction coefficient of μ_s = 0.15 was assumed following studies on scaling effects [13]. For contact definition ***CONTACT_FORMING_SURFACE_TO_SURFACE** was used. The austenitic stainless steel X2CrNiMo17 12 2 (1.4404) with a sheet thickness of t_0 = 0.1 mm was used as a typical representative material used in proton-exchange membrane fuel cell applications. An anisotropic material model according to Barlat [14] (***MAT_133**) was parameterized based on quasi-static and dynamic tensile tests as well as bulge tests.

3 Optimization of model boundary conditions for efficient process simulation

3.1 Evaluation criteria and permissible limits

The simulation of the hollow embossing rolling process of the introduced test geometry already requires a total of 4 h 58 min for an mpp calculation with 32 CPUs using conventional mass scaling. According to the CPU load distribution, the contact calculation (49%) and the calculation of the deformable shell elements of the strip section (18%) dominate (Fig. 3b). For subsequent investigations, the test geometry was further reduced due to the already high computation time and a miniaturized variant was derived for fast computable qualitative comparative simulations (Fig. 3a). This reduced the computational time to 1 h 15 min (25%) for the same boundary conditions.

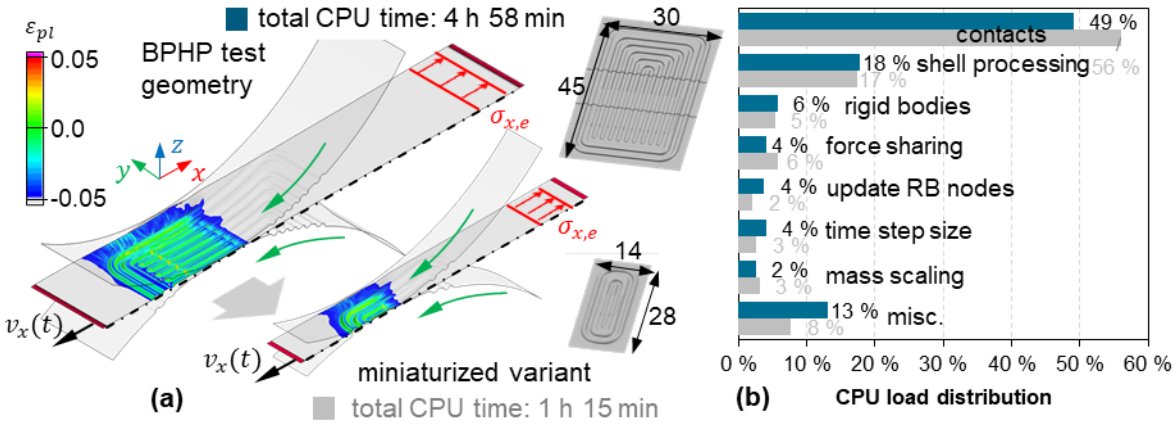

Fig.3: (a) derivation of a miniaturized test geometry and (b) analysis of the CPU load distribution.

Several approaches to reduce model computation time are discussed below. The objective of the simulation studies is to find a balance between computational time savings and model errors due to simplified model approaches. Result change evaluation is performed by analyzing various technologically relevant criteria, where the standard deviations S are primarily used for result estimation, in addition to the maximum deviations. Table 1 lists the evaluation criteria considered and the assumed permissible limits of the standard deviation S_{lim}. These limits were set at a level that still allows the corresponding change in results to be considered irrelevant from a technological point of view. To evaluate any potential effects on the springback results and flatness deviation from the reference geometry, an implicit springback simulation is carried out after each forming simulation of the rolling process. The flatness deviation was determined in each case by best-fit converting the strip mesh into the corresponding nominal geometry in CATIA© V5.

Evaluation criteria	**Symbol**	**Corresponding limit value of standard deviation S_{lim}**
difference in strip thickness in longitudinal and transversal cross section	Δt	$S_{\Delta t,lim}$ = 0.001 mm (≙ 1% of t_0)
difference in true plastic strain in longitudinal and transversal cross section	$\Delta\varepsilon_{pl}$	$S_{\Delta\varepsilon,lim}$ = 0.01
difference in rolling force in z-direction	ΔF	$S_{\Delta F,lim}$ = 2% (related to the maximum force value of the reference model)
difference in z-displacement of discrete nodes	Δz	$S_{\Delta z,lim}$ = 0.02 mm
difference in flatness deviation to the target geometry	Δgeo	$S_{\Delta geo,lim}$ = 0.01 mm (≙ 10% of t_0)

Table 1: Evaluation criteria of model deviation and corresponding standard deviation.

3.2 Influence of mass scaling and process time acceleration

In order to reduce the computation time, both an accelerated calculation of the process (time acceleration $\eta = t_{virtual} / t_{real}$) and the use of mass scaling by larger explicit time steps dt is a proven means of conventional sheet metal forming simulation using LS-DYNA©. Based on the reference model, discrete time acceleration factors (η = 1 – 20) and time step sizes without ($dt = 1 \cdot 10^{-8}$ s) as well as with

conventional mass scaling dt_{MS} and selective mass scaling dt_{SMS} (dt = 3 · 10^{-8} – 3 · 10^{-7} s) were tested and evaluated with respect to the result changes of the evaluation criteria using the miniaturized test geometry. In the following, the case without acceleration (η = 1) and without mass scaling (dt = 1 · 10^{-8} s), for which the computation time is about 74 h, serves as a reference case without corresponding effects influencing model accuracy. Fig. 4 shows the changes in results (standard deviation S and permissible limits S_{lim} on the secondary ordinate) for different variants of η and dt compared to the reference case also including the achievable reduction in CPU time (primary ordinate).

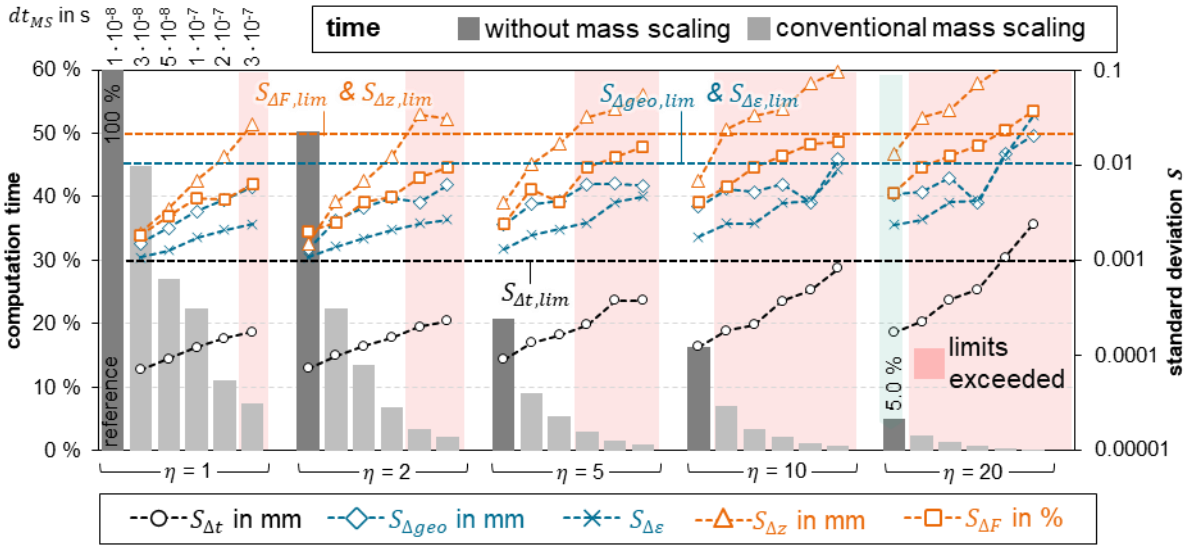

Fig.4: Influence of conventional mass scaling and process time acceleration on CPU time and standard deviation of evaluation criteria differences.

For exclusive process time acceleration (dt = 1 · 10^{-8} s), the calculation time can be reduced to 5% (~ 3.7 h) of the reference value with η = 20 ($v_{virtual}$ = 2200 mm/s). For η > 20, the limit of the permissible nodal displacement $S_{\Delta z,lim}$ is exceeded. Slight increases in the time step size dt_{MS} in the course of conventional mass scaling affect all evaluation criteria in the form of increasing values of the standard deviations S. The sensitivity seems to increase with increasing process time acceleration. In particular, the change of $S_{\Delta z}$ is already so significant at η = 20 that no further savings are possible compared to the case without mass scaling. With the alternative use of selective mass scaling, the standard deviations change slightly and the assumed limits are not exceeded as quickly as in the case with conventional mass scaling (Fig. 5).

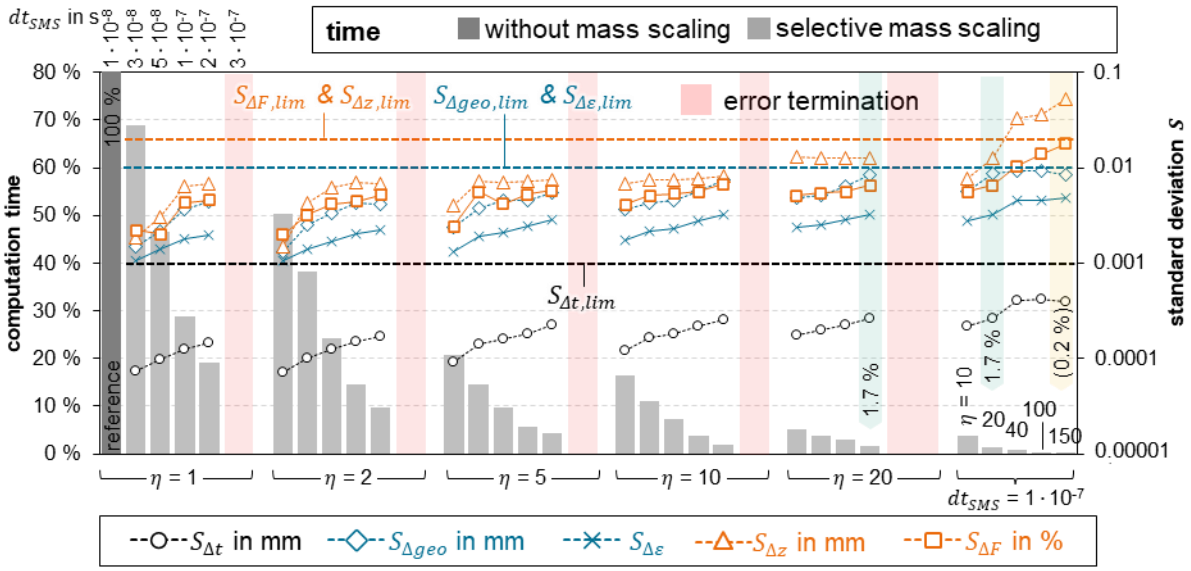

Fig.5: Influence of selective mass scaling and process time acceleration on CPU time and standard deviation of evaluation criteria differences.

With η = 20 and dt_{SMS} = 1 · 10^{-7} s, the computation time can be reduced to 1.7% of the reference case (~ 75 min) while respecting the limits of all evaluation criteria considered. For $dt_{SMS} \geq 2 \cdot 10^{-7}$ s, contact problems increasingly occur and the simulations sometimes terminate prematurely, so that no further savings can be realized by even larger time step sizes dt_{SMS}. For significantly larger BPHP geometries, a higher process time acceleration η can be considered to further decrease the calculation time. By accepting the demonstrated model errors of nodal displacement in the z-direction ($S_{\Delta z}$), it is possible to achieve additional computation time savings while adhering to the limits of all other evaluation criteria. In the comparison case, the calculation time is reduced to 0.2% of the reference case (9 min) for dt_{SMS} = 1 · 10^{-7} s and η = 150 ($v_{virtual}$ = 16500 mm/s).

3.3 Strip meshing and shell modeling

Selecting a mesh fine enough to achieve precise local resolution of the bending and strain deformations without significantly increasing the number of elements and computational effort is the main challenge when modeling the forming processes of fine channel structures in BPHP. For the sake of efficient modeling, and in contrast to other published articles, shell element discretization of the strip section is used intentionally because the model approach presented should also be suitable for industry-relevant BPHP sizes in dimensions of 400 x 200 mm. The respective channel cross-section could be simulated using two-dimensional models as well, which is still useful, particularly for an initial assessment of forming feasibility. Since flatness deviation of the complete BPHP is of particular interest for process evaluation, mapping the entire BPHP in forming and springback simulation is mandatory.

The comparison study considers the following parameters: element edge length l_e, shell element type E_T (ELFORM in ***SECTION_SHELL**), and the number of shell integration points n_{IP}. The goal was to study interactions and identify the best adjustment parameters, while dealing with the tradeoff between computational time and model accuracy. The combinations of strip meshing parameters, as seen in Fig. 6, were analyzed initially without the use of adaptive mesh refinement. The time step size dt_{SMS} was modified with element edge length ensuring consistent boundary conditions regarding selective mass scaling. The reference is established by combining the values of l_e = 0.05 mm, E_T = 16, and n_{IP} = 9 (5 h 35 min). Approximately 8 shell elements with l_e = 0.05 mm map the minimum tool radius R0.25 found here. For l_e = 0.075 and 0.10 mm, respectively, only 5 and 4 shell elements extend over the smallest radius.

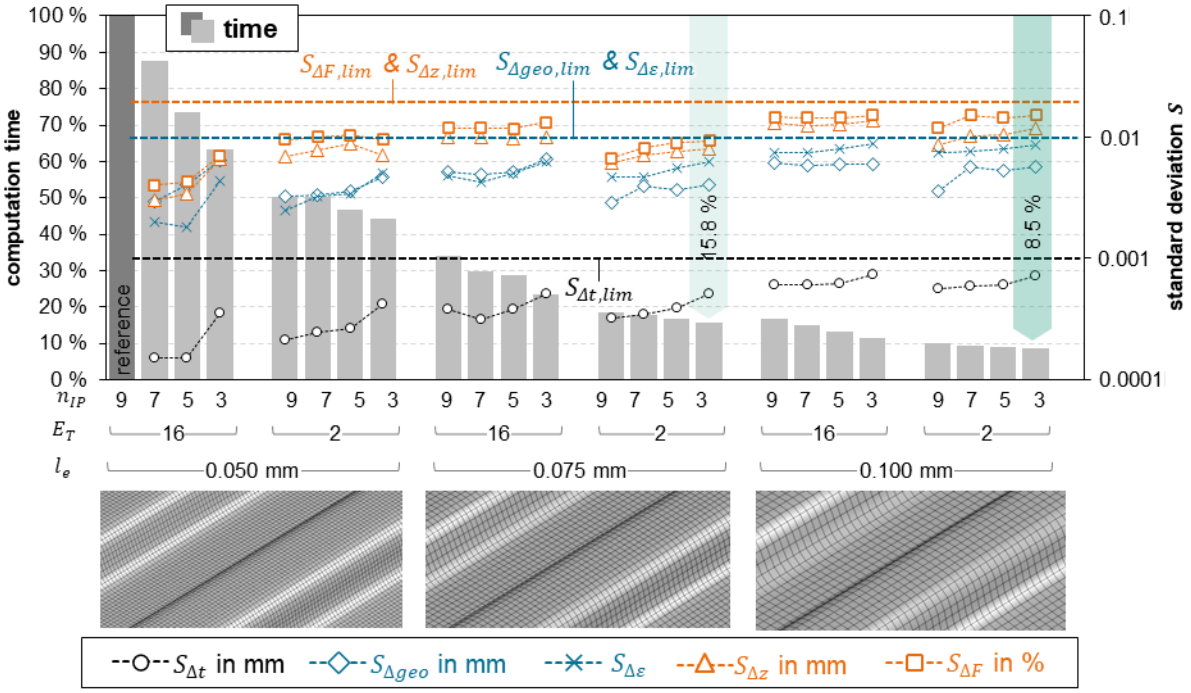

Fig.6: Influence of strip element length and meshing parameters on CPU time and standard deviation of evaluation criteria differences.

The comparisons indicate that the standard deviation limits are exceeded when l_e > 0.10 mm. Regardless of the other investigated discretization parameters, this comparatively coarse meshing of the strip leads to an inadequate representation of channel forming. The standard deviation limits are

met at l_e = 0.10 mm, and clearly undercut at l_e = 0.075 mm. Increasing the number of integration points n_{IP} is expected to result in a more detailed modeling of stresses and strains across shell thickness, which in turn can enable resolution of the effects caused by bending deformation with greater precision. The standard deviations $S_{\Delta t}$ and $S_{\Delta \varepsilon}$ tend to increase as n_{IP} decreases. Nevertheless, there is only a minor change in the results of each case with the same element type. Thus, selecting a high number of integration points is not likely to result in a considerable decrease of the model error. Instead, it may significantly increase the computation time required. Therefore, selecting n_{IP} = 3 for modeling of hollow embossing rolling on thin strips is justified since it only contributes to a negligible additional model error in comparison to the reference case. Changing from E_T = 16 (fully integrated shell) to E_T = 2 (reduced integrated shell), standard deviations of the evaluation criteria do not show a clear trend for constant values of n_{IP}. Sensitivities of the standard deviations are relatively low here, so a decision can be made in favor of a less time-intensive model approach to enhance model efficiency. On average, using E_T = 2 instead of E_T = 16 in the performed comparative calculations can reduce element calculation time to 26%. In summary, the parameter combination of l_e = 0.075 mm, E_T = 2, and n_{IP} = 3 is recommended for the geometrical boundary conditions present here (R0,25). Compared to an equivalent simulation with l_e = 0.10 mm, this results in an 86% increase in computational time. The associated changes in the results are well below the set limits, and, on average, 30% lower compared to l_e = 0.10 mm. With 32 CPUs, the calculation time can be reduced to 53 min, which corresponds to 15.8% of the reference case (l_e = 0.05 mm, E_T = 16, n_{IP} = 9).

Adaptive mesh refinement is generally a promising method for efficient sheet metal forming simulations, providing an alternative to initial uniformly fine shell meshing. Adaptive mesh refinement is also well-suited for incremental forming in hollow embossing rolling. However, the advantage of adaptive mesh refinement may be limited due to the time-consuming reinitialization resulting from the out-of-core h-adaptivity in mpp calculations [15]. Conventional one-pass h-adaptivity (***CONTROL_ADAPTIVE**: ADPTOL = 1°, 50 adaptivity steps during forming process, MAXLVL = 2) and predictive mesh refinement based on tool surface curvature (ADPENE = 2, ADPTOL = 1°, 10 adaptivity steps during forming process, MAXLVL = 2) were evaluated after separate identification of adaptivity parameters to identify possible optimization opportunities. Comparing the results to the respective reference simulations without adaptivity, conventional h-adaptivity presents significant calculation time savings, as expected. However, it is also associated with a considerable change in results. For instance, using l_e = 0.15 mm and only one refinement level (MAXLVL = 2, $l_{e,min}$ = 0.075 mm), h-adaptive mesh refinement can decrease the computation time from 15.8% (reference case with initially fine strip mesh l_e = 0.075 mm) to 10.7%. However, the standard deviations of the evaluation criteria increase significantly due to the h-adaptive mesh refinement. This causes the model error level to almost match that of uniform initial strip mesh with l_e = 0.10 mm without refinement (computation time 8.5%). A further refinement level cannot be recommended here due to the limit values being exceeded. The saving potential of computation time with h-adaptive mesh refinement is 20% lower in total than with a simulation without refinement and slightly larger element edge length (l_e = 0.10 mm) for the same resulting model error. This confirms that coventional h-adaptive mesh refinement is not advantageous for mpp calculations with many CPUs [16].

Predictive adaptivity based on tool surface curvature results in lower standard deviations from the reference than conventional h-adaptive mesh refinement with the same boundary conditions. The mesh refinement does not start by advancing strip bending but is initiated before tool contact. However, the potential savings in computation time are also reduced in comparison, since mesh refinement is typically more extensive and earlier, which provides more elements in the strip mesh. Despite using predictive mesh refinement, the ratio of model error to computation time savings cannot be decisively improved. Current developments in in-core h-adaptivity are promising and may unlock further saving potentials in the future [17].

3.4 Roller surface meshing

As with the strip mesh, the discretization of the rigid roll segments is not only a factor that affects the accuracy of the model, but also the computation time. In general, a sufficiently fine tool mesh should be aimed at for exactly reproducing the macroscopic curvature of the roll segments on the one hand and to represent the channel geometries on the other hand. A typical practice in forming simulations with LS-DYNA© is to use a tool surface meshing with 8 – 10 elements over the smallest tool radius. With a minimum tool radius of R0.25, this results in an element edge length of l_e = 0.04 – 0.05 mm. Fig. 7 provides a summary of the simulation studies considering different rigid roller surface meshes. The roller meshing was executed by using the Auto-Mesher in LS-PREPOST©. In the beginning, roller meshes

with almost square elements ($l_{e,max}$ = $l_{e,min}$) were derived, and later meshes were generated with $l_{e,max}$ > $l_{e,min}$. In the latter situation, meshes with axial-stretched elements $l_{e,max}$ can be created by setting a low angle criterion. These meshes will still conform to $l_{e,min}$ in the tangential direction as well as in the channel radius regions. Thus, the number of elements for the roller segments can be significantly decreased, which positively impacts the computation time. The simulations were performed assuming a uniform strip mesh where l_e was set to 0.075 mm.

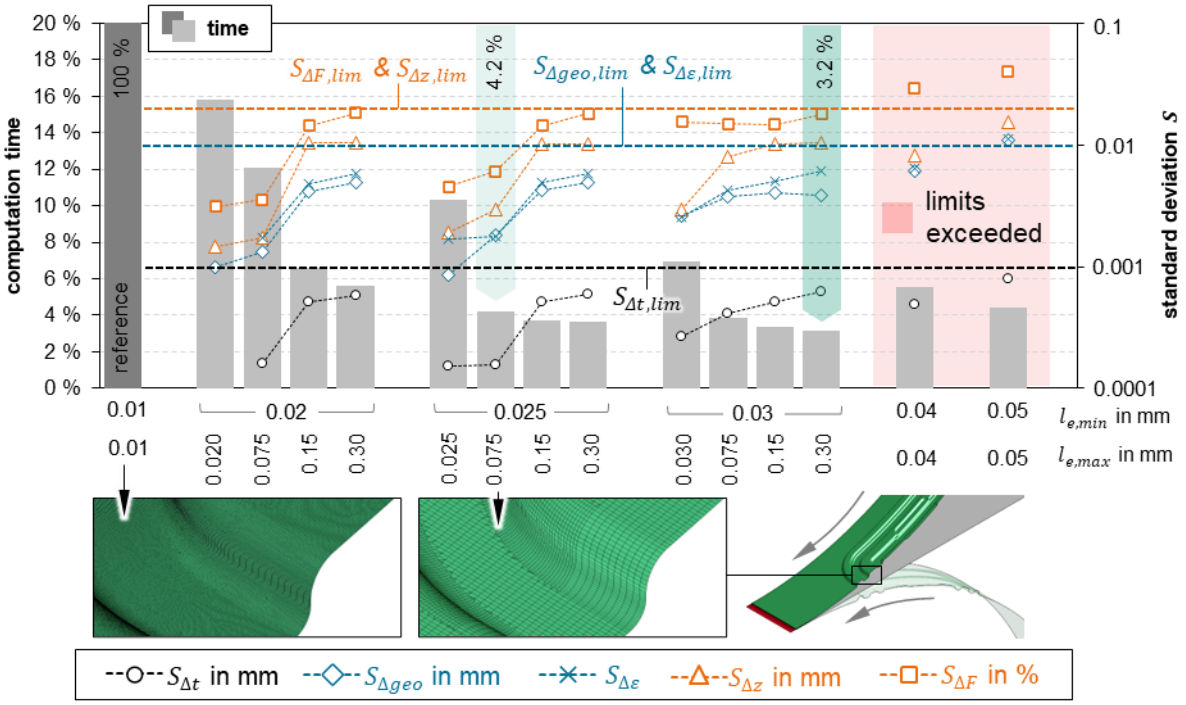

Fig.7: Influence of tool surface meshing parameters on CPU time and standard deviation of evaluation criteria differences.

The comparative calculations demonstrate increasing result standard deviations and decreasing calculation times as the edge lengths with square elements are uniformly increased from 0.01 mm (reference) to 0.05 mm. From l_e = 0.04 mm, changes of rolling force standard deviation $S_{\Delta F}$ exceed the permissible limits due to the coarse roller mesh. When the minimum element edge length $l_{e,min}$ is set constant, stepwise increasing of $l_{e,max}$ results in axially stretched elements and significantly decreased computation times. However, all evaluation criteria considered show increasing result deviations compared to the reference case. The changes in standard deviations between $l_{e,max}$ = 0.075 mm and 0.15 mm is substantial. The case with $l_{e,min}$ = 0.025 mm and $l_{e,max}$ = 0.075 mm offers the best balance of model efficiency, reducing computational time to 4.2% of the reference value while having only a minimal impact on model error.

4 Summary

This paper introduces a shell-based FE model for representing hollow embossing rolling in LS-DYNA© to model the forming process of bipolar half-plates (BPHP) by rolling processes. A miniaturized variant based on a BPHP test geometry with typical discontinuous channel structures was derived for several comparative simulations. The aim of this was to quantify the influence of different setting parameters (time acceleration, mass scaling, meshing, and discretization parameters) on the associated model error and the feasible computation time savings. The results of the simulation studies are summarized in Table 2. In the final evaluation, the ratio of the standard deviation to the permissible limit value was listed as a percentage for all evaluation criteria. A process time acceleration of η = 20 leads to a small model error for the assumed boundary conditions (20 rpm, D = 105 mm) and is therefore recommended as a conservative approach. Then, the virtual strip speed is $v_{virtual}$ = 2,200 mm/s. Applying selective mass scaling can reduce calculation time even further by using dt_{SMS} = 1 · 10^{-7} s, and the average change in simulation results increases only slightly (from S/S_{lim} = 36% to 48%). Even greater computation time savings are feasible with $\eta \leq 150$ ($v_{virtual}$ = 16,500 mm/s) as a progressive approach requiring acceptance of increasing result changes in nodal displacements ($S_{\Delta z}$).

	S/S_{lim}						computation time
	ΔF	Δz	$\Delta \varepsilon$	Δgeo	Δt	average	
time acceleration and mass scaling, reference: η = 1, dt_{MS} = 1 · 10^{-8} s							100%
η = 20, dt_{MS} = 1 · 10^{-8} s, konv.	26%	66%	24%	49%	17%	**36%**	**5.0%**
η = 20, dt_{MS} = 1 · 10^{-7} s, selektiv	33%	62%	32%	85%	27%	**48%**	**1.7%**
η = 150, dt_{MS} = 1 · 10^{-7} s, selektiv	90%	263%	48%	86%	36%	**105%**	**0.2%**
Strip meshing and discretization, reference: l_e = 0.05 mm, E_T = 16, n_{IP} = 9							100%
l_e = 0.075 mm, E_T = 2, n_{IP} = 3	47%	40%	63%	40%	51%	**48%**	**15.8%**
l_e = 0.10 mm, E_T = 2, n_{IP} = 3	76%	59%	87%	56%	72%	**70%**	**8.5%**
l_e = 0.15 – 0.075 mm, E_T = 2, n_{IP} = 3, h-adaptive	86%	67%	77%	58%	62%	**70%**	**10.7%**
rigid tool surface meshing, reference l_e = 0,01 mm							100%
$l_{e,min}$ = 0.025, $l_{e,max}$ = 0.075 mm	30%	15%	18%	18%	16%	**19%**	**4.2%**
$l_{e,min}$ = 0.030, $l_{e,max}$ = 0.300 mm	89%	53%	60%	38%	62%	**60%**	**3.2%**

Table 2: Summary of the resulting result deviations (standard deviations) and computation time savings for the model approaches considered.

For metal strip discretization, it is recommended to use a uniform initial element edge length of l_e = 0.075 mm as a conservative approach, considering the given boundary conditions of the BPHP geometry (minimum tool radius R0.25). Using a finer value of l_e = 0.10 mm leads to an increase in the averaged standard deviation from 48% to 70% of the limit values. However, it also reduces the CPU time by 46% compared to l_e = 0.075 mm. The utilization of adaptive mesh refinement as an alternative has been studied and found to be disadvantageous for the assumed mpp calculation. Based on the comparative simulation studies, it could further be deduced that shell element formulation ELFORM = 2 with 3 integration points has sufficient accuracy and provides a marginal model error from a technological point of view. For rigid roller surface meshing, it is recommended to use variable mesh sizes with $l_{e,min}$ = 0,025 mm and $l_{e,max}$ = 0,075 mm providing efficient roller meshes with lower model error.

5 Literature

[1] Federal Ministry for Economic Affairs and Energy: The National Hydrogen Strategy. URL: https://www.bmwk.de/Redaktion/EN/Publikationen/Energie/the-national-hydrogen-strategy.pdf?__blob=publicationFile&v=6. retrieval date: 22.03.2023.

[2] Riemer, M.; Zheng, L.; Eckstein, J.; Wietschel, M.; Pieton, N.; Kunze, R.: Future hydrogen demand: A cross-sectoral, global meta-analysis. HYPAT Working Paper 04/2022. URL: https://www.isi.fraunhofer.de/content/dam/isi/dokumente/cce/2022/HYPAT_Working_Paper_04_2022_Future_hydrogen_demand.pdf. retrieval date: 22.03.2023.

[3] Hung, J.-C.; Lin, C.-C.: Fabrication of micro-flow channels for metallic bipolar plates by a high-pressure hydroforming apparatus. In: Journal of Power Sources 206 (2012), pp. 179–84.

[4] Bong, H. J.; Lee, J.; Kim, J.-H.; Barlat, F.; Lee, M.-G.: Two-stage forming approach for manufacturing ferritic stainless steel bipolar plates in PEM fuel cell: Experiments and numerical simulations. In: International Journal of Hydrogen Energy 42 (2017) 10, pp. 6965–77.

[5] Porstmann, S.; Wannemacher, T.; Drossel, W.-G.: A comprehensive comparison of state-of-the-art manufacturing methods for fuel cell bipolar plates including anticipated future industry trends. In: Journal of Manufacturing Processes 60 (2020), pp. 366–83.

[6] Nikam, V.; Reddy, R.: Corrugated bipolar sheets as fuel distributors in PEMFC. In: International Journal of Hydrogen Energy 31 (2006) 13, pp. 1863–73.

[7] Abeyrathna, B.; Zhang, P.; Pereira, M. P.; Wilkosz, D.; Weiss, M.: Micro-roll forming of stainless steel bipolar plates for fuel cells. In: International Journal of Hydrogen Energy 44 (2019) 7, pp. 3861–75.

[8] Bauer, A.; Härtel, S.; Awiszus, B.: Manufacturing of Metallic Bipolar Plate Channels by Rolling. In: Journal of Manufacturing and Materials Processing 3 (2019) 2, pp. 48.

[9] Bauer, A.: Experimentelle und numerische Untersuchungen zur Analyse der umformtechnischen Herstellung metallischer Bipolarplatten, Dissertation. Chemnitz 2020.

[10] Porstmann, S., Polster, S., Reuther, F., Melzer, S., Nagel, M., Psyk, V., Dix, M.: Objectives and fields of tension in the comparison of manufacturing processes for metallic bipolar plates. Chemnitz 2021.
[11] Huang, J.; Deng, Y.; Yi, P.; Peng, L.: Experimental and numerical investigation on thin sheet metal roll forming process of micro channels with high aspect ratio. In: The International Journal of Advanced Manufacturing Technology 100 (2019) 1-4, pp. 117–29.
[12] Fiedler, M.; Kittner, K.; Awiszus, B.: Production of Metallic Bipolar Plates Made of Stainless Steel by Incremental Hollow Embossing Using Rollers: The 28th Saxon Conference on Forming Technology SFU and the 7th International Conference on Accuracy in Forming Technology ICAFT. Basel Switzerland.
[13] Vollertsen, F.; Hu, Z.: Tribological Size Effects in Sheet Metal Forming Measured by a Strip Drawing Test. In: CIRP Annals 55 (2006) 1, pp. 291–94.
[14] Barlat, F.; Brem, J. C.; Yoon, J. W.; Chung, K.; Dick, R. E.; Lege, D. J.; Pourboghrat, F.; Choi, S.-H.; Chu, E.: Plane stress yield function for aluminum alloy sheets—part 1: theory. In: International Journal of Plasticity 19 (2003) 9, pp. 1297–319.
[15] Fan, H.; Wainscott, B.; Zhang, L.; Zhu X.: Performance Study of In Core Adaptivity in LS-DYNA 2020.
[16] Dutton, T.; Weinschenk, A.: Optimising Run Times for Sheet Metal Forming Simulation 2020.
[17] Wainscott, B.; Fan, H.: In Core Adaptivity. Detroit 2018.